



**HAL**  
open science

## **Structural insights into the interaction between testis-specific Y-encoded-like protein 5 and ubiquitin-specific protease 7**

Marine Ancia, Khadija Wahni, Joudy Chakrowf, Asia El Aakchioui, Eloïse Claude, Guillaume de Lhoneux, Maxime Liberelle, Steven Janvier, Ekaterina Baranova, Julia Malo Pueyo, et al.

### ► **To cite this version:**

Marine Ancia, Khadija Wahni, Joudy Chakrowf, Asia El Aakchioui, Eloïse Claude, et al.. Structural insights into the interaction between testis-specific Y-encoded-like protein 5 and ubiquitin-specific protease 7. *Protein Science*, 2025, 34 (5), pp.e70116. <10.1002/pro.70116>. <hal-05221470>

**HAL Id: hal-05221470**

**<https://hal.science/hal-05221470v1>**

Submitted on 25 Aug 2025

**HAL** is a multi-disciplinary open access archive for the deposit and dissemination of scientific research documents, whether they are published or not. The documents may come from teaching and research institutions in France or abroad, or from public or private research centers.

L'archive ouverte pluridisciplinaire **HAL**, est destinée au dépôt et à la diffusion de documents scientifiques de niveau recherche, publiés ou non, émanant des établissements d'enseignement et de recherche français ou étrangers, des laboratoires publics ou privés.



HAL Authorization

1 Structural Insights into the Interaction Between Testis-Specific  
2 Y-Encoded-Like Protein 5 and Ubiquitin-Specific Protease 7

3  
4 Marine Ancia<sup>1,2</sup>, Khadija Wahni<sup>3,4,5</sup>, Joudy Chakrowf<sup>1</sup>, Asia El Aakchioui<sup>1</sup>, Eloïse  
5 Claude<sup>2</sup>, Guillaume de Lhoneux<sup>2</sup>, Maxime Liberelle<sup>1#</sup>, Steven Janvier<sup>3,5</sup>, Ekaterina  
6 Baranova<sup>3,4,5</sup>, Julia Malo Pueyo<sup>3,4,5</sup>, Ariana Jijon Vergara<sup>1</sup>, Nicolas Papadopoulos<sup>7,8</sup>,  
7 Clémence Balty<sup>7,9</sup>, Jérôme Dejeu<sup>6</sup>, Anabelle Decottignies<sup>2</sup>, Joris Messens<sup>3,4,5\*</sup> and  
8 Raphaël Frédérick<sup>1\*</sup>

9  
10 1. Medicinal Chemistry Research Group, Louvain Drug Research Institute,  
11 Université catholique de Louvain, B-1200 Brussels, Belgium

12 2. Genetic and Epigenetic Alterations of Genomes, de Duve Institute, Faculty of  
13 Pharmacy and Biomedical Sciences, Université catholique de Louvain,  
14 Brussels 1200, Belgium

15 3. VIB-VUB Center for Structural Biology, Vlaams Instituut Voor Biotechnologie,  
16 B-1050 Brussels, Belgium

17 4. Brussels Center for Redox Biology, Vrije Universiteit Brussel, B-1050  
18 Brussels, Belgium

19 5. Structural Biology Brussels, Vrije Universiteit Brussel, B-1050 Brussels,  
20 Belgium

21 6. Université Marie et Louis Pasteur, SUPMICROTECH, CNRS, institut FEMTO-  
22 ST, 25000 Besançon, France

23 7. de Duve Institute, Université catholique de Louvain, Brussels, Belgium

24 8. Ludwig Institute for Cancer Research, Brussels, Belgium

25 9. IONS/NEUR, Université Catholique de Louvain, Brussels, Belgium  
26 #. Present address: University of Lille, Lille Neurosciences and Cognition  
27 Research Center, U1172, Lille, France

28

29 \* Corresponding authors:

30 Raphaël Frédérick (raphael.frederick@uclouvain.be) (+32 2 7647341)

31 Joris Messens (Joris.Messens@vub.be) (+32 2 6291992)

32

33

34 **Running title:** Structural Insights into the TSPYL5-USP7 Interaction

35

36 **Table of content:**

37 Manuscript pages: 1-39

38 Supplementary material pages: S1-S28

39 Figures: Fig. 1 - Fig. 5

40

41 **TSPYL5-USP7-supplementary-material:** Complementary results about  
42 immunoprecipitation assay, mass spectrometry experiments, structure prediction,  
43 hydrogen-deuterium exchange mass spectrometry experiments, proteins production  
44 and analysis, BioLayer Interferometry assay, peptides screening, sequence  
45 comparison and hotspots localization, dynamic light scattering and mass photometry  
46 experiments, and Materials and Methods Tables.

47

48

49

50 **ABSTRACT**

51

52 The Alternative Lengthening of Telomeres (ALT) mechanism enables telomere  
53 maintenance, contributing to the immortality of certain cancer cells. Disrupting the  
54 interaction between Testis-Specific Y-encoded-like Protein 5 (TSPYL5) and Ubiquitin-  
55 Specific Protease 7 (USP7) has emerged as a promising strategy to target ALT-  
56 dependent cancers. While the N-terminal MATH domain of USP7 mediates the protein  
57 interaction, the regions of TSPYL5 involved in binding remain unclear. Here, we  
58 present a structural analysis of the TSPYL5-USP7 interaction to guide targeted  
59 therapeutic strategies. We showed that TSPYL5 is intrinsically disordered, with an  
60 unfolded N-terminal region and partial structure in the C-terminal half. *In vitro*,  
61 recombinantly expressed TSPYL5 binds USP7 with nanomolar affinity and was prone  
62 to C-terminal truncation. However, the truncated form retained a similar binding affinity  
63 for USP7, suggesting the primary interaction site resides in the N-terminal region of  
64 TSPYL5. We identified three key binding hotspots within TSPYL5: residues 65-97,  
65 residues 210–262, and residues 368–388. Moreover, TSPYL5 forms trimers that  
66 further assemble into hexamers. This study provides the first structural and quantitative  
67 analysis of the TSPYL5-USP7 interaction, highlighting these three binding sites. These  
68 findings lay the groundwork for the development of novel inhibitors targeting ALT-  
69 dependent cancers.

70

71

72

73

74

75 **Keywords:**

76 ALT mechanism, cancer, co-immunoprecipitation, microscale thermophoresis,  
77 bilayer interferometry, hydrogen-deuterium exchange mass spectrometry, peptides  
78 screening, AlphaFold, mass photometry, electron microscopy

79

80

81 **A 50-75-word statement, written for a broader audience, outlining the importance**  
82 **and/or impact of the work presented in the manuscript:**

83 The interaction between TSPYL5 and USP7 is critical for the survival of cancer cells  
84 that use the Alternative Lengthening of Telomeres (ALT) mechanism for telomere  
85 maintenance —common in many solid pediatric tumors. By identifying key regions  
86 involved in this interaction, our findings offer a foundation for developing targeted  
87 therapies that could disrupt ALT in cancer cells, providing a promising new approach  
88 for treating these challenging cancers.

89

90

91

92

93

94

95

96

97

98

99

## 100 INTRODUCTION

101

102 Cellular immortality, a hallmark of cancer (Hanahan and Weinberg 2011), is often  
103 achieved through the maintenance of telomere length. Cancer cells typically utilize one  
104 of two primary mechanisms for telomere elongation: the reactivation of telomerase via  
105 the re-expression of the *hTERT* telomerase gene, or the activation of the Alternative  
106 Lengthening of Telomeres (ALT) mechanism, which involves homologous  
107 recombination-based telomere maintenance (Claude and Decottignies 2020; Zhang  
108 and Zou 2020).

109 While telomerase is reactivated in approximately 85% of cancers, ALT is particularly  
110 prevalent in certain tumor types, such as sarcomas, neuroblastomas, and central  
111 nervous system tumors, where it occurs in 50-60% of cases. Importantly, around one-  
112 third of solid pediatric tumors are ALT-dependent (Claude and Decottignies 2020).  
113 Current pediatric cancer treatments often cause severe side effects because of their  
114 aggressiveness and non-specificity (Forrest et al. 2018). Targeting ALT offers a  
115 promising strategy for developing more specific and less toxic therapies, as the  
116 pathway is inactive in normal cells. However, therapeutic interventions targeting ALT  
117 remain challenging, as this pathway relies on canonical homologous recombination  
118 DNA repair pathways, which complicates the development of selective inhibitors.  
119 Despite these difficulties, several key features of ALT are being investigated as  
120 potential targets (Zhang and Zou 2020).

121 The Testis-Specific Y-encoded-like Protein 5 (TSPYL5) recently emerged as a putative  
122 therapeutic target against ALT-positive (ALT<sup>+</sup>) tumors, as it is essential for the survival  
123 of ALT<sup>+</sup> cells, including SV40T-immortalized fibroblasts and sarcoma cells (Episkopou  
124 et al. 2019). Depletion of TSPYL5 selectively induces ALT<sup>+</sup> cell death, without affecting

125 the viability of telomerase-positive cells or normal skin fibroblasts, providing a strong  
126 rationale for targeting this protein in ALT<sup>+</sup> tumors (Episkopou et al. 2019).  
127 Mechanistically, ALT<sup>+</sup> cell death induced by TSPYL5 depletion was found to result from  
128 the interaction of TSPYL5 with the Ubiquitin-Specific Protease 7 (USP7). The depletion  
129 of TSPYL5 leads to the degradation of the Protection of Telomeres 1 (POT1)  
130 component of the shelterin complex, triggering DNA damage responses and cell death  
131 (Episkopou et al. 2019). Given the importance of the TSPYL5-USP7 interaction in ALT<sup>+</sup>  
132 cancer cell survival, targeting this protein-protein interaction represents an attractive  
133 therapeutic strategy for ALT-dependent cancers.

134 USP7, a deubiquitinating enzyme, is known to interact with TSPYL5 through its TRAF-  
135 like or MATH domain (Epping et al. 2011), but the interacting region of TSPYL5  
136 remains unknown. TSPYL5, a member of the TSPY-like protein family, is characterized  
137 by a high degree of intrinsic disorder (65.7% of predicted intrinsically disordered  
138 regions (IDRs)), which likely contributes to its propensity for liquid-liquid phase  
139 separation (LLPS) (Silonov et al. 2024). Evidence suggests its involvement in various  
140 cellular functions, such as nucleosome assembly (Dalui et al. 2022) or modulation of  
141 p53 levels (Epping et al. 2011). However, the structural features of TSPYL5 and how  
142 it interacts with USP7 remain poorly explored.

143 In this study, we sought to identify the key interaction sites between TSPYL5 and  
144 USP7. By characterizing the structural properties of TSPYL5, quantifying its binding  
145 affinity for USP7, and mapping the interacting regions through cellular assays and  
146 peptide screening, we aim to provide crucial insights that could guide the development  
147 of targeted therapies to disrupt this interaction, offering a promising approach for  
148 treating ALT-dependent pediatric tumors.

149

## 150 **RESULTS**

151

### 152 **The N-terminal region of TSPYL5 interacts with USP7 in pull-down assays**

153 To study the TSPYL5-USP7 interaction and identify potential binding hotspots on  
154 TSPYL5, we designed constructs for the overexpression of either full-length TSPYL5  
155 (FL) or three distinct segments of TSPYL5 in human cells. The last 174 amino acids of  
156 TSPYL5, predicted to form a NAP-like domain, were included in TSPYL5 #3 (residues  
157 243–417) (Fig. 1A-B). The remaining sequence was divided into two regions: TSPYL5  
158 #1 (residues 1–123), corresponding to the N-terminal part predicted to be unfolded,  
159 and TSPYL5 #2 (residues 124–242), which includes the remaining unfolded region and  
160 a predicted  $\alpha$ -helix (Fig. 1A-B). Each construct (FL, #1, #2, and #3) was fused to an N-  
161 terminal triple-Flag tag (Fig. 1A).

162 Flag immunoprecipitation assays were performed using lysates from U2OS cells (Fig.  
163 1C) or HEK293T cells (Fig. S1) overexpressing these constructs. As expected, Flag-  
164 TSPYL5 FL efficiently co-immunoprecipitated USP7, confirming their interaction. Flag-  
165 TSPYL5 #1 also pulled down USP7, indicating that this part of TSPYL5 mediates the  
166 interaction. Additionally, Flag-TSPYL5 #2, which includes the predicted  $\alpha$ -helix, also  
167 recovered USP7, indicating an additional interaction site within this region. In contrast,  
168 Flag-TSPYL5 #3, corresponding to the C-terminal region, failed to pull down USP7  
169 (Fig. 1C). These findings suggest that the C-terminal region of TSPYL5 does not  
170 participate in USP7 binding, while the N-terminal part plays a key role in the interaction.

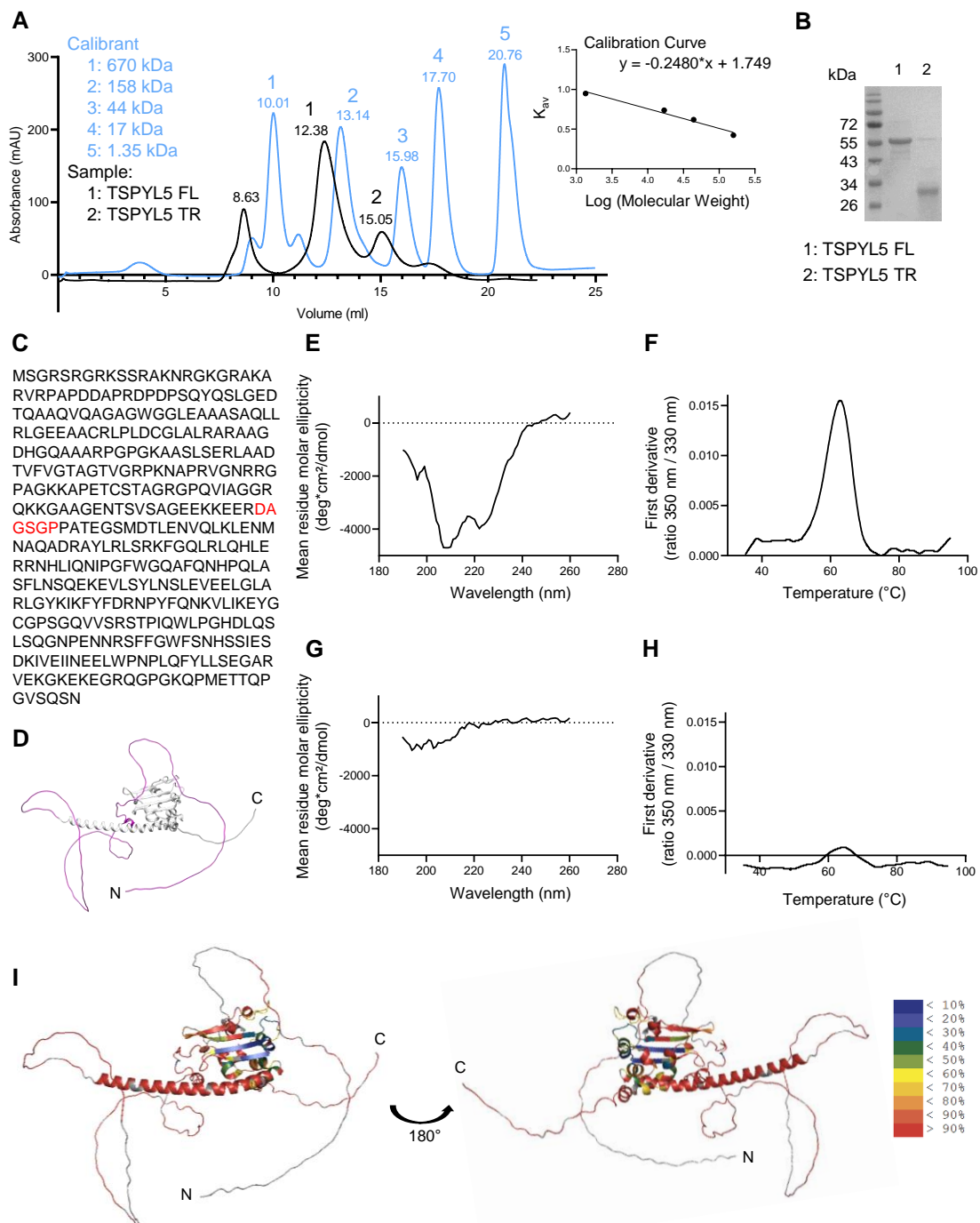


## 186 TSPYL5 is a partially folded protein

187 To further investigate the TSPYL5-USP7 interaction, we expressed full-length human  
188 TSPYL5 in *E. coli* (SoluBL21) and purified the protein using nickel resin and size  
189 exclusion chromatography (SEC) (Fig. 2A). Two distinct forms were obtained: full-  
190 length TSPYL5 (TSPYL5 FL), eluting at 12.38 ml (peak 1), and a truncated form  
191 (TSPYL5 TR), eluting at 15.05 ml (peak 2). Both proteins were highly pure, as  
192 confirmed by SDS-PAGE (Fig. 2B). SEC analysis determined the molecular weight  
193 (MW) of TSPYL5 FL to be around 360 kDa, suggesting oligomer formation, while mass  
194 spectrometry indicated a 47 kDa mass (Fig. S2A). The truncated form (TSPYL5 TR, 1-  
195 195 residues) had a measured MW of 21 kDa, with a potential cleavage site identified  
196 (Fig. 2C, Fig. S2B-E). Structural predictions from AlphaFold2 (Jumper et al. 2021;  
197 Varadi et al. 2024) suggested that the truncated form (highlighted in pink on the grey  
198 TSPYL5 FL structure) is largely unfolded (Fig. 2D). Circular dichroism (CD) and nano  
199 differential scanning fluorimetry (nanoDSF) analysis revealed TSPYL5 FL exhibits at  
200 least partial folding, with an  $\alpha$ -helical and  $\beta$ -sheet content (two minima near 208 nm  
201 and 222 nm) (Fig. 2E) and a melting temperature of 63.2°C (Fig. 2F). In contrast,  
202 TSPYL5 TR showed profiles typical of unfolded proteins, consistent with structural  
203 predictions (Fig. 2G, H).

204 To further probe TSPYL5 FL structure, we performed hydrogen-deuterium exchange  
205 mass spectrometry (HDx-MS) experiments. HDx-MS provides insights into solvent  
206 accessibility and secondary structure, as exchange rates vary with structural context:  
207 they are fastest in disordered regions (random coils), intermediate in  $\alpha$ -helices, and  
208 slowest in  $\beta$ -sheets (Weis 2016). The HDx-MS data (Fig. 2I) revealed that most of  
209 TSPYL5 exchanges deuterium rapidly, suggesting a predominantly flexible and  
210 disordered conformation. However, variations in exchange rates were observed in  
211 regions predicted to form  $\beta$ -sheets and  $\alpha$ -helices, largely aligning with the AlphaFold2  
212 structural model. Notably, some discrepancies between the predicted and  
213 experimentally determined secondary structure were observed. For example,  
214 AlphaFold2 predicts a  $\beta$ -sheet for residues NSLEVEEL, whereas HDx-MS suggests  
215 that the  $\beta$ -sheet extends to residues (VL)SYLNSLEV, preceding the predicted region.  
216 Additional discrepancies can be deduced from Fig. S3.

217



219

220 **Figure 2: TSPYL5 adopts a partially structured conformation and spontaneously cleaves into a**  
 221 **predominantly unfolded form. (A)** Size exclusion chromatography (SEC) profile of TSPYL5 (black  
 222 curve) during the purification process displays an elution volume of 12.38 ml (peak 1) (TSPYL5 FL),  
 223 corresponding to an estimated molecular weight of ~360 kDa, based on a calibration curve (standard  
 224 protein elution profile in light blue). A smaller species elutes at 15.05 ml (peak 2), corresponding to a

225 truncated form of TSPYL5 (TSPYL5 TR). Elution volumes are indicated above the peaks. The calibration  
226 curve was generated using proteins of known molecular weight ( $K_{av}$  is the distribution coefficient, slope  
227  $SE = 0.02872$ , Y-intercept  $SE = 0.1254$ ); the first peak of the calibration profile was excluded due to  
228 exceeding the column's separation range. **(B)** SDS-PAGE analysis shows the molecular weights and  
229 purity of TSPYL5 FL and TR eluting in peaks 1 and 2, respectively. **(C)** Mass spectrometry analysis  
230 identifies the potential cleavage site (highlighted in red) on the TSPYL5 construct sequence (details in  
231 Figure S2). **(D)** AlphaFold2 representation of TSPYL5 TR (highlighted in pink), corresponding to the N-  
232 terminus of the full-length protein superimposed on TSPYL5 FL structure. "N" refers to the N-terminus  
233 and "C" to the C-terminus. **(E)** Circular dichroism analysis of TSPYL5 FL (0.2 mg/ml). **(F)** Thermal  
234 denaturation profile of TSPYL5 FL, measured by nano Differential Scanning Fluorimetry (nanoDSF)  
235 (Melting Temperature = 63.2°C). **(G)** Circular dichroism analysis of TSPYL5 TR (0.2 mg/ml). **(H)** Thermal  
236 denaturation profile of TSPYL5 TR, measured by nanoDSF (uncalculated Melting Temperature). **(I)**  
237 Hydrogen-deuterium exchange mass spectrometry (HDx-MS) analysis of TSPYL5 FL. The H-D  
238 exchange percentage at 60 s is mapped onto the AlphaFold2-predicted TSPYL5 structure. Color coding  
239 indicates exchange dynamics: high exchange (red) denotes flexible, disordered regions, while lower  
240 exchange suggests the presence of secondary structures, including  $\beta$ -sheets (blue) and  $\alpha$ -helices  
241 (yellow/green).

242

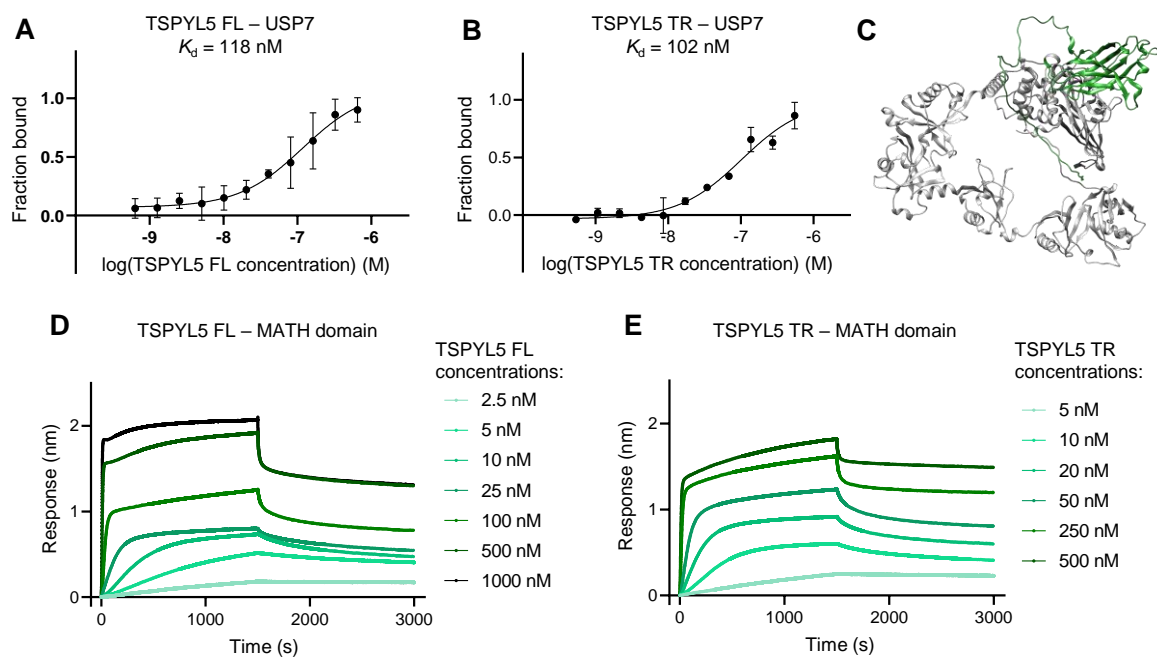
### 243 **Both TSPYL5 FL and TR bind strongly to USP7**

244 To investigate the interaction between TSPYL5 and USP7, we measured their binding  
245 affinity using Microscale Thermophoresis (MST). Building on previous  
246 immunoprecipitation data showing that the N-terminal half of TSPYL5 interacts with  
247 USP7 in human cells, we used the naturally occurring truncated TSPYL5 (TSPYL5 TR)  
248 form to further explore the role of the N-terminal region in mediating this interaction.  
249 MST binding analyses confirmed that USP7 binds to full-length TSPYL5 (TSPYL5 FL),  
250 with a dissociation constant ( $K_d$ ) of 118.1 nM (Fig. 3A). In line with the cellular data,

251 TSPYL5 TR also demonstrated strong binding to USP7 with a  $K_d$  of 102.4 nM (Fig.  
252 3B).

253 To validate these findings with an orthogonal method, we employed BioLayer  
254 Interferometry (BLI). Previous co-immunoprecipitation (co-IP) studies identified the  
255 MATH domain of USP7 as the key region mediating its interaction with TSPYL5  
256 (Epping et al. 2011). Given that USP7 is a large protein, we decided to focus on its  
257 MATH domain (Fig. 3C). We successfully expressed and purified the USP7 MATH  
258 domain and confirmed its proper folding (Fig. S4A-D). In our initial BLI experiments,  
259 we attempted to titrate the MATH domain in solution using biotinylated TSPYL5 FL  
260 immobilized on streptavidin-coated sensors. However, we found that immobilizing  
261 TSPYL5 on the sensor likely obstructed its binding site, yielding inconclusive results  
262 (see supplementary material for more details, Fig. S5). In contrast, immobilization of  
263 the MATH domain after biotinylation produced clear and conclusive data (Fig. 3D and  
264 E). Kinetic analysis of TSPYL5 binding to the MATH domain revealed association ( $k_{on}$ )  
265 and dissociation ( $k_{off}$ ) rates of around  $1.3 \times 10^5 \text{ M}^{-1}\text{s}^{-1}$  and around  $3.4 \times 10^{-4} \text{ s}^{-1}$ ,  
266 respectively (Fig. 3F, Fig. S6), yielding a mean  $K_d$  of 3.4 nM. Similarly, the MATH  
267 domain exhibited comparable affinity for TSPYL5 TR, with a mean  $K_d$  of 2.1 nM.

268



Protein immobilized on the sensor	Interacting partner	$K_d$ from kinetic analysis
Biotinylated MATH domain	TSPYL5 FL	1.7 - 5.1 nM $k_{on} = 7.0 \times 10^4 - 1.9 \times 10^5$ 1/M.s $k_{off} = 3.2 \times 10^{-4} - 3.6 \times 10^{-4}$ 1/s
Biotinylated MATH domain	TSPYL5 TR	0.8 - 3.3 nM $k_{on} = 7.2 \times 10^4 - 2.1 \times 10^5$ 1/M.s $k_{off} = 1.7 \times 10^{-4} - 2.4 \times 10^{-4}$ 1/s

269

270 **Figure 3: USP7 and its MATH domain interact strongly with both full-length and truncated**  
 271 **TSPYL5.** (A) Microscale thermophoresis binding curve for TSPYL5 FL, ranging from 650 nM to 0.635  
 272 nM, with a constant concentration of USP7 (100 nM), yields a dissociation constant ( $K_d$ ) of 118 nM (95%  
 273 CI [85 nM – 164 nM], N=3, mean  $\pm$  SD). (B) Microscale thermophoresis binding curve for TSPYL5 TR,  
 274 ranging from 550 nM to 0.537 nM, with USP7 at a constant concentration (100 nM), results in a  $K_d$  of  
 275 102 nM (95% CI [55 nM – 201 nM], N=2, mean  $\pm$  SD). (C) AlphaFold2 prediction of the USP7 structure,  
 276 highlighting the MATH domain in green in the N-terminal region. (D) Kinetic BioLayer Interferometry  
 277 binding curves for TSPYL5 FL at various concentrations with a constant concentration of biotinylated

278 MATH domain (2.5  $\mu\text{g/ml}$ ). TSPYL5 FL is added at  $t = 0$  s and washed at  $t = 1500$  s. (E) Kinetic BioLayer  
279 Interferometry binding curves for TSPYL5 TR at various concentrations with a constant concentration  
280 of biotinylated MATH domain (2.5  $\mu\text{g/ml}$ ). TSPYL5 TR is added at  $t = 0$  s and washed at  $t = 1500$  s. (F)  
281 Determined affinity values for the binding of TSPYL5 FL and TR with the MATH domain of USP7 by  
282 BioLayer Interferometry (N=2; each value represents a replicate). See supplementary material for more  
283 details (Fig. S6).

284

### 285 **Three key hotspots mediate the interaction between TSPYL5 and USP7**

286 To investigate the primary interaction sites between TSPYL5 and USP7, we first  
287 identified key interaction regions within the TSPYL5 #1 and #2 sequences (Fig. 1C).  
288 We then conducted hydrogen-deuterium exchange mass spectrometry (HDx-MS)  
289 experiments with TSPYL5 and the MATH domain of USP7 to pinpoint specific  
290 interaction hotspots on the TSPYL5 sequence. This analysis covered 85.6% of the  
291 TSPYL5 sequence, enabling an in-depth examination of the binding across most of the  
292 protein (Fig. S7). Differential H-D exchange analysis revealed two major regions of  
293 TSPYL5 with significantly reduced deuterium uptake in the presence of the USP7  
294 MATH domain. The first region spans residues ~210–262, while the second region  
295 covers residues ~368–388 at 15 and 60 s of exchange (Fig. 4A–B, Fig. S8–9).

296 To further refine the identification of interaction sites, we performed a peptide  
297 screening approach, which is particularly useful for mapping protein-protein interaction  
298 regions in unfolded proteins. We divided the 417 amino acids of TSPYL5 FL into 51  
299 overlapping 17-amino-acid peptides, each overlapping by 9 residues, to ensure  
300 comprehensive sequence coverage (Fig. 4C). MST screening identified three  
301 overlapping peptides (peptides 9, 10, and 11) in the N-terminal region of TSPYL5 that  
302 bound to USP7, with dissociation constants ( $K_d$ ) ranging from 12.6  $\mu\text{M}$  to 500  $\mu\text{M}$  (Fig.

303 4D–E, Table S2). These peptides map to amino acids 65–97 of TSPYL5, suggesting  
304 this region forms a key interaction hotspot. The localization of these three peptides  
305 within the TSPYL5 #1 sequence further supports the findings from cellular  
306 experiments. However, this region was not detected in HDx-MS experiments,  
307 presumably due to the very fast exchange kinetics in this region, which prevented the  
308 observation of differential deuterium exchange at the shortest time point tested (15 s),  
309 by which these peptides had already fully exchanged (Fig. S3).

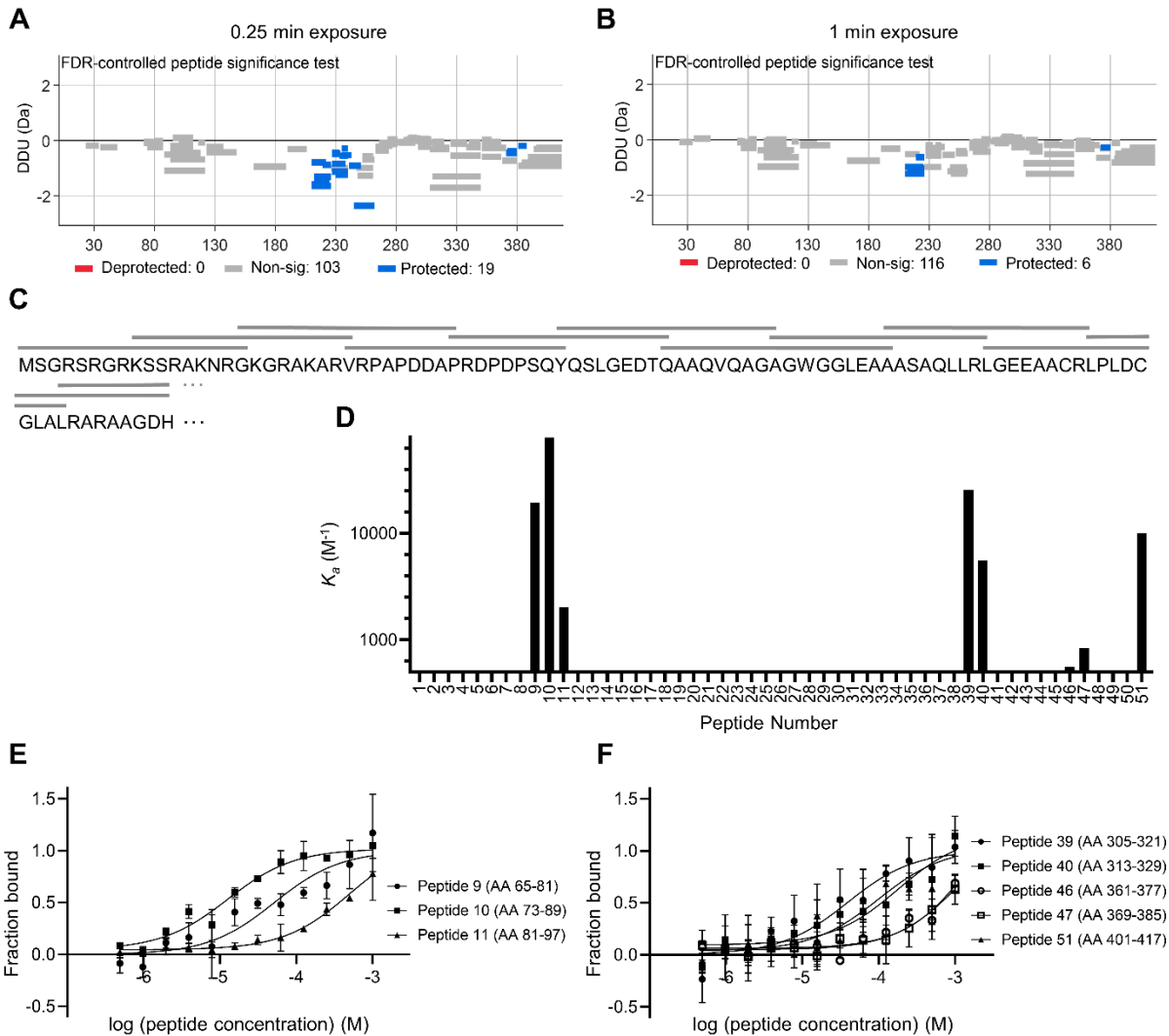
310 Additionally, five interacting peptides were identified in the C-terminal region of  
311 TSPYL5 (Fig. 4D-F). The region corresponding to peptides 46 and 47 was also  
312 detected in HDx-MS, with these two peptides displaying low-affinity binding (Fig. 4D–  
313 F, Table S3). This low binding affinity may explain why TSPYL5 #3 failed to co-  
314 immunoprecipitate with USP7 in our cellular experiments. Among the five interacting  
315 peptides in the C-terminal region, only peptides 46 and 47 were validated by an  
316 orthogonal technique, designating them as confirmed interaction hotspots. The  
317 remaining peptides showed no detectable interaction, even at concentrations up to 1  
318 mM (Fig. 4D, Table S2-3). Notably, no binding was observed for peptides from the first  
319 region identified by HDx-MS (residues ~210–262), likely due to the lack of a defined  
320 structural conformation of peptides, as this region is predicted to form an  $\alpha$ -helix, which  
321 may be important for interaction. Overall, our experiments identified three key  
322 interaction hotspots: hotspot 1 in the N-terminal region (amino acids 65–97), hotspot 2  
323 in the central region (amino acids 210–262) and hotspot 3 in the C-terminal region  
324 (amino acids 368–388).

325 To explore the evolutionary significance of the identified hotspots, we compared the  
326 human TSPYL5 sequence to those of other species (Fig. S10A). As expected, the  
327 NAP-like domain of TSPYL5 (underlined in orange) is highly conserved across

328 species. The three identified interaction hotspots (highlighted in pink) also displays  
329 notable conservation, suggesting their functional importance. A comparison of human  
330 TSPYL5 with other TSPYL family members (Fig. S10B) showed conservation of the  
331 NAP-like domain, whereas the N-terminal region, including the sequence  
332 corresponding to peptides 9, 10, and 11, exhibited significant divergence across family  
333 members. In contrast, the sequences corresponding to hotspots 2 and 3 displayed  
334 similarity across TSPYL family members, indicating potential functional overlap within  
335 the family.

336

337



338

339 **Figure 4: Three key hotspots were identified for the TSPYL5-USP7 interaction.** (A-B) Differential  
 340 hydrogen-deuterium exchange (HDx) analysis identifies TSPYL5 peptides that exhibit protection or  
 341 deprotection upon MATH domain binding. Significantly protected peptides (peptide significance test,  $p$   
 342  $< 0.01$  (Lau et al. 2021)) are shown in blue after 0.25 min (A) and 1 min (B) of deuterium exposure (FDR  
 343 = false discovery rate, DDU = differential deuterium uptake). (C) Schematic representation of the  
 344 TSPYL5 peptides used in the screening process, focusing on the N-terminal region of TSPYL5. Each  
 345 gray line represents an individual peptide. (D) Affinity constants ( $K_a = 1/K_d$ ) obtained from Microscale  
 346 Thermophoresis (MST) for the 51 TSPYL5 peptides screened against USP7. USP7 concentration was  
 347 held constant (100 nM), while peptide concentrations ranged from 1 mM to 488 nM. Absence of a value  
 348 indicates undetectable binding (N=2 for most peptides, N=3 for interacting peptides; detailed data in  
 349 Table S2-3).  $K_a$  or  $K_d$  values for peptides 46 and 47 should be interpreted with caution, as the measured

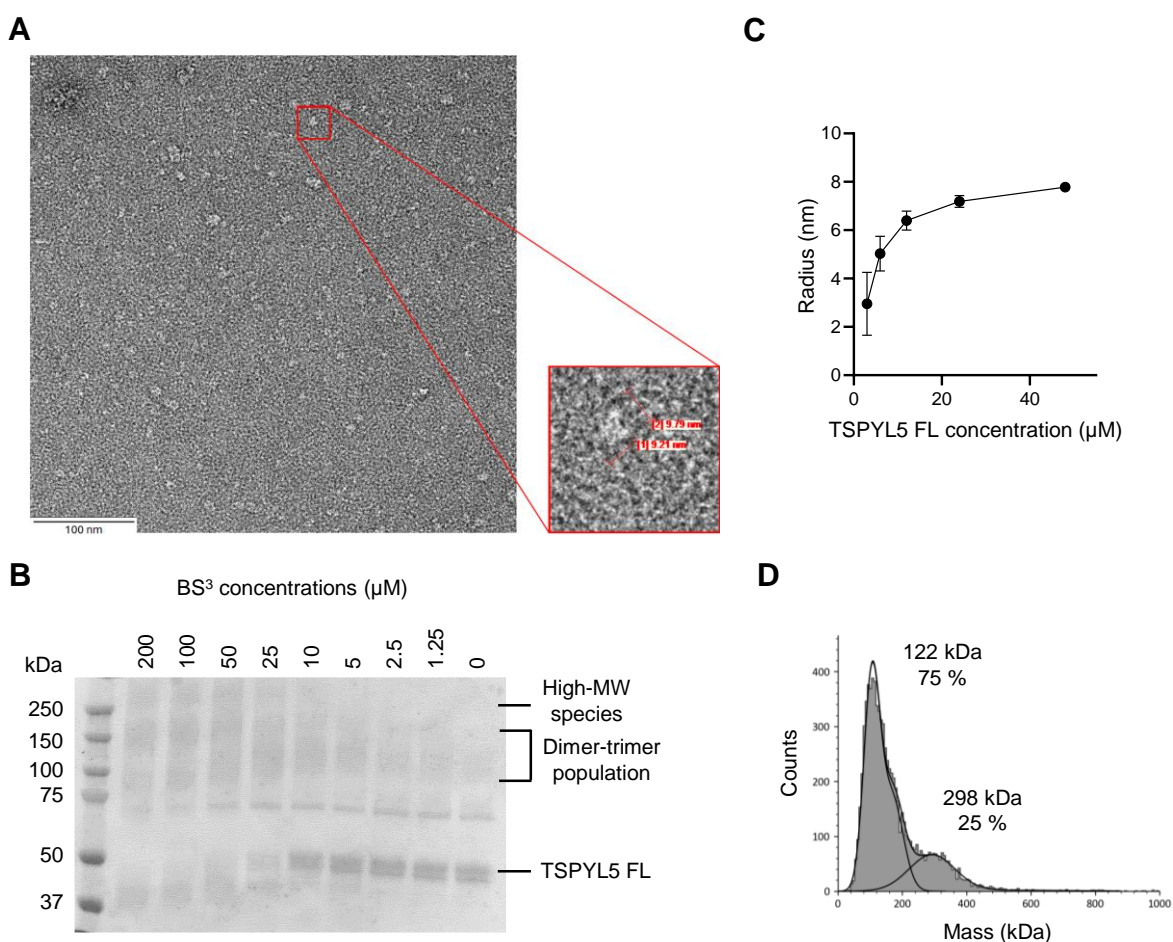
350  $K_d$  exceeds the highest tested peptide concentration. (E-F) MST binding curves for detected interacting  
351 peptides shown in D, with amino acid boundaries indicated in parentheses (N=3, mean  $\pm$  SD).

352

### 353 **TSPYL5 assembles into trimers and hexamers**

354 To further investigate TSPYL5, we performed negative staining electron microscopy,  
355 which revealed a heterogeneous population of particles, predominantly around 9 nm  
356 in size (Fig. 5A). This finding supports the high-MW species observed in our SEC  
357 analysis (Fig. 2A). To explore the oligomerization mechanism, we conducted a  
358 crosslinking assay with the BS<sup>3</sup> (Bis(Sulfosuccinimidyl) suberate) crosslinker. As the  
359 crosslinker concentration increased, the monomeric TSPYL5 band gradually  
360 disappeared, while multiple higher-MW bands appeared, indicating oligomer formation  
361 (Fig. 5B). Due to the size and complexity of the resulting bands, precise MW  
362 determination was challenging. Therefore, we used Dynamic Light Scattering (DLS)  
363 and Mass Photometry (MP) for a more detailed analysis of TSPYL5 in solution. DLS  
364 measurements showed that at higher concentrations (~50  $\mu$ M), TSPYL5 forms 8 nm  
365 complexes (Fig. 5C), consistent with the 9 nm particles seen in electron microscopy.  
366 DLS also revealed a reduction in particle size as the protein concentration decreased  
367 (Fig. 5C, Fig. S12A), aligning with the crosslinking data suggesting the existence of  
368 multiple oligomeric states. Mass photometry, which provides accurate MW  
369 determination at low concentrations (~ 80 nM), identified a trimer (~120 kDa) and its  
370 dimerization to form a hexamer (~300 kDa) (Fig. 5D). Collectively, these results confirm  
371 that TSPYL5 assembles into hexamers (~300 kDa, 8–9 nm in diameter) at higher  
372 concentrations (~50  $\mu$ M). Additionally, we observed that the hexamer formation occurs  
373 via an intermediate trimer, which becomes more predominant at lower concentrations  
374 (Fig. S12B).

375 To gain deeper insights into the oligomerization process of TSPYL5, we examined its  
 376 truncated form (TSPYL5 TR, residues 1-195). Mass spectrometry determined its  
 377 molecular weight (MW) to be 21 kDa, but size exclusion chromatography (SEC)  
 378 analysis indicated a MW of ~65 kDa, suggesting trimer formation (Fig. 2A). To explore  
 379 this further, we produced and purified an anti-truncated version of TSPYL5 (TSPYL5  
 380 anti-TR, residues 196-417) (Fig. S13A). Nano differential scanning fluorimetry  
 381 (nanoDSF) analysis confirmed that TSPYL5 anti-TR is at least partially folded, with a  
 382 melting temperature of 51.1°C (Fig. S13B). SEC analysis indicated an apparent MW  
 383 of ~62 kDa, while its actual MW was ~28 kDa (Fig. S13C), suggesting dimerization.  
 384 These findings imply that the N-terminal region of TSPYL5 plays a crucial role in trimer  
 385 formation, while the C-terminal region likely mediates the interaction of two trimers,  
 386 leading to hexamer formation.



387

388 **Figure 5: TSPYL5 forms trimers and hexamers.** (A) Negative staining electron microscopy of purified  
389 TSPYL5 FL (0.01 mg/ml), with a zoom (in red) on a 9 nm diameter particle. (B) Crosslinking experiment:  
390 TSPYL5 FL was incubated at 3.5  $\mu$ M with increasing concentrations of BS<sup>3</sup> and results were analyzed  
391 with SDS-PAGE. (C) Dynamic light scattering analysis of TSPYL5 FL at different concentrations (mean  
392  $\pm$  SD, N=2, n=6). (D) Mass photometry experiment of TSPYL5 FL at a low concentration (77 nM), with  
393 the calculated molecular weights of the complexes in solution and their relative abundance indicated  
394 next to the peaks.

395

## 396 **DISCUSSION**

397

398 The interaction between TSPYL5 and USP7 has emerged as a promising target for  
399 anti-ALT therapy, particularly in the context of pediatric cancers that rely on the ALT  
400 mechanism for telomere maintenance (Episkopou et al. 2019). However, the  
401 mechanistic details of this interaction remain poorly understood, limiting the  
402 development of effective therapeutic strategies. In this study, we characterized the  
403 interaction between full-length (FL) TSPYL5 and USP7, shedding light on key aspects  
404 of this interaction.

405

406 Our cell-based assays revealed that the N-terminal half of TSPYL5 mediates its  
407 interaction with USP7, while no binding was observed with the C-terminal half  
408 (residues 243–417), which includes the NAP-like domain. This suggests that the NAP-  
409 like domain does not play a significant direct role in USP7 binding. These findings were  
410 further supported by *in vitro* binding assays, confirming that the N-terminal region of  
411 TSPYL5, which is predicted to be disordered, is crucial for its interaction with USP7.  
412 Additionally, our binding hotspot analysis identified a specific interaction site within this

413 C-terminal region, albeit with low affinity, which likely explains why it failed to co-  
414 immunoprecipitate with USP7.

415

416 In line with previous studies (Silonov et al. 2024), our structural analysis confirmed that  
417 TSPYL5 is an intrinsically disordered protein, with its N-terminal region lacking a stable  
418 secondary structure. This structural flexibility likely contributes to its ability to engage  
419 in dynamic protein-protein interactions. Interestingly, we also observed the  
420 spontaneous formation of a truncated TSPYL5 form (TSPYL5 TR) during protein  
421 production, which we speculate reflects the structural instability of the full-length  
422 protein.

423

424 We used Microscale Thermophoresis (MST) to quantify the interaction between  
425 TSPYL5 and USP7, and the resulting dissociation constant of 118 nM for the full-length  
426 protein indicates high-affinity binding. The TSPYL5 TR form also exhibited similar  
427 binding affinity, suggesting that the interaction hotspot located within the disordered  
428 N-terminal region plays a major role in the binding. When we focused on the MATH  
429 domain of USP7, the binding affinity was even stronger (~3 nM), suggesting that the  
430 full-length USP7 may have structural constraints that reduce the accessibility of the  
431 MATH domain to TSPYL5. These results highlight the importance of the MATH domain  
432 in the TSPYL5-USP7 interaction and point to the need for further structural studies to  
433 understand how other USP7 domains may influence this interaction.

434

435 Peptide screening revealed a critical hotspot for the interaction between TSPYL5 and  
436 USP7 spanning amino acids 65 to 97 in the N-terminal region. However, hydrogen-  
437 deuterium exchange experiments failed to confirm this site, likely due to the rapid

438 exchange dynamics in this intrinsically disordered region, which prevented detectable  
439 differences under our experimental conditions. This region is highly conserved in  
440 TSPYL5 across species, suggesting its functional importance. Interestingly, the human  
441 TSPYL family members show some divergence in this region, which could explain why,  
442 except for TSPYL1 (Oughtred et al. 2021), they do not interact with USP7. This  
443 variability may indicate that the interaction between TSPYL5 and USP7 is specific to  
444 TSPYL5, while TSPYL1 may use distinct binding mechanisms.

445 Furthermore, our analysis of the TSPYL5 #2 fragment (residues 124–242) showed that  
446 it interacts with USP7 in cell-based assays. This was confirmed through HDx-MS  
447 experiments, which identified a binding hotspot within the  $\alpha$ -helix spanning amino acids  
448 210 to 262. However, no binding was detected in our *in vitro* peptide screening. This  
449 discrepancy suggests that the structured  $\alpha$ -helix within this fragment may not be well-  
450 represented in the peptide screening model, as it does not preserve the native  
451 conformation of the full-length protein.

452 Previous studies have identified a consensus sequence (P/A/E-x-x-S) for the binding  
453 of the MATH domain of USP7 to various targets (Kim and Sixma 2017). The absence  
454 of this consensus in the identified TSPYL5 hotspots suggests that TSPYL5 interacts  
455 with USP7 via a unique mechanism. This is consistent with previous observations that  
456 TSPYL5 functions as an inhibitor of USP7, rather than as a substrate (Epping et al.  
457 2011). Additionally, the fact that USP7 binds to some substrates at two distinct sites  
458 (Ma et al. 2010) further supports the idea that TSPYL5 may engage USP7 in a non-  
459 canonical manner, distinct from other USP7 substrates.

460

461 The unexpectedly similar  $K_d$  values observed for TSPYL5 TR and FL, despite the  
462 truncation occurring just before the  $\alpha$ -helix, were intriguing. We speculate that a single,

463 strong binding hotspot in the N-terminal region could be sufficient to maintain the  
464 overall interaction, ensuring high affinity even in the absence of additional interaction  
465 sites. This hypothesis is further supported by the peptide screening results, where  
466 peptides 9, 10, and 11 exhibited lower  $K_d$  values compared to other identified peptides.  
467 Alternatively, the structural characteristics of TSPYL5 TR may enhance the  
468 accessibility or stability of this hotspot, leading to comparable binding affinities despite  
469 the truncated form having fewer interaction regions. This suggests that cooperative  
470 effects between different binding sites could contribute to the overall affinity, as  
471 previously suggested (de Vink et al. 2022).

472

473 We also observed that TSPYL5 forms oligomeric species in solution, with trimers and  
474 hexamers being the predominant forms at lower and higher concentrations,  
475 respectively. The N-terminal region appears to drive trimer formation, while the C-  
476 terminal region likely promotes hexamer formation by the interaction of two trimers.  
477 This oligomerization behavior is consistent with previous reports that the C-terminal  
478 region of TSPYL5 can self-assemble (Dalui et al. 2022), as well as with findings from  
479 related proteins like TSPY1, which require oligomerization for function (Shen et al.  
480 2018). These results suggest that TSPYL5 may rely on oligomerization for its full  
481 functional activity, which could be an important consideration when developing  
482 targeted inhibitors.

483

484 In conclusion, this study provides a detailed characterization of the TSPYL5-USP7  
485 interaction, identifying key binding hotspots and revealing the structural basis for this  
486 interaction. The high-affinity binding observed between TSPYL5 and USP7,  
487 particularly within the disordered N-terminal region, offers a promising target for the

488 development of specific inhibitors. These inhibitors could selectively kill ALT-positive  
489 cancer cells, potentially offering a more specific and less toxic therapeutic option.  
490 Furthermore, our findings on the oligomerization behavior of TSPYL5 open new  
491 avenues for designing strategies that target its oligomeric state. Together, these  
492 insights provide a strong foundation for the development of peptide- or small molecule-  
493 based inhibitors with minimal off-target effects, paving the way for the next generation  
494 of anti-ALT therapies.

495

496

## 497 **MATERIALS AND METHODS**

498

499 **Chemicals and reagents.** All reagents were obtained from commercial suppliers, as  
500 detailed below, and were used without further purification.

501

502 **DNA constructs.** The complementary DNA encoding TSPYL5 full length or different  
503 constructs was generated by PCR from the pBABE-puro-1xFlag-Nbio-TSPYL5  
504 retroviral plasmid (Table S4) using forward and reverse primers (Table S5). The PCR  
505 products were subsequently cloned into the pCDNA-3xFLAG-NLS-TPP1 plasmid  
506 (Table S4). All final constructs were confirmed by DNA sequencing.

507

508 **Cell culture.** The *in vitro* immortalized human embryonic kidney cell line, HEK293T  
509 (ATCC CRL-3216), as well as the osteosarcoma cell line, U2OS (ATCC HTB-96), were  
510 cultured in DMEM (41965039, Gibco) supplemented with 10% FBS (F7524, Sigma-

511 Aldrich) and 1% penicillin-streptomycin (17602E, Lonza), under 37°C / 5% CO<sub>2</sub>  
512 conditions.

513

514 **Transfection.** Cells were seeded in 6-well plates with a density of 0.15 million  
515 cells/well and incubated overnight (ON) before transfection. Per well, 1 µg of plasmid  
516 (Table S4) and 4 µg of PEI 25K™ (23966, Polysciences Inc.) were mixed in 200 µL of  
517 serum-free medium (31985047, Gibco) and incubated at room temperature (RT) for 20  
518 min before incubation with the cells for 6 h in 1.8 mL medium supplemented with 10%  
519 FBS. After the 6 h incubation, the medium was discarded and replaced with fresh  
520 supplemented medium.

521

522 **Immunoprecipitations and western blotting.** Cells were washed two times with ice-  
523 cold phosphate-buffered saline (PBS) and lysed for 30 min in NP-40 lysis buffer (50  
524 mM Tris-HCl pH 7.4, 1 mM EDTA pH 8, 75 mM NaCl, 0.5 % NP-40) supplemented  
525 with protease inhibitors (11836153001, Roche). Lysates were centrifuged at 12,000 ×  
526 g for 10 min at 4°C, supernatants were collected and heated for 10 min at 95°C in 6×  
527 Laemmli buffer (300 mM Tris-HCl pH 6.8, 60% glycerol, 12% sodium dodecyl sulphate  
528 (SDS) and 0.03% bromophenol blue, completed with 0.1 M dithiothreitol (DTT)).  
529 Alternatively, for immunoprecipitations, 500 µg of proteins were incubated overnight at  
530 4°C with 20 µL of anti-Flag M2 affinity gel (A2220, Sigma-Aldrich). Immunoprecipitates  
531 were washed three times in cold NP-40 wash buffer (50 mM Tris-HCl pH 7.4, 1 mM  
532 EDTA pH 8, 75 mM NaCl, 0.1% NP-40), and beads were eluted and heated for 3 min  
533 at 95°C in 6× Laemmli buffer. Western blotting was performed according to standard  
534 procedures using antibodies described in Table S6. Revelation was performed with  
535 SuperSignal West Pico Chemiluminescent Substrate (ThermoFisher Scientific).

536

## 537 **Proteins production and purification**

538 *TSPYL5*. The nucleotidic sequence encoding *TSPYL5*, modified to include an N-  
539 terminal 6x histidine tag followed by a thrombin cleavage site, was cloned into the pET-  
540 28a expression vector and synthesized by Genecust. The recombinant plasmid was  
541 transformed into *Escherichia coli* SoluBL21 cells. Transformed *E. coli* cultures were  
542 grown in terrific broth (TB) supplemented with 50 µg/mL kanamycin at 37°C. Protein  
543 expression was induced by adding 1 mM isopropyl β-D-1-thiogalactopyranoside  
544 (IPTG) when the culture reached an optical density (OD<sub>600</sub>) of 0.8. The cultures were  
545 incubated overnight at 20°C with shaking at 120 rpm. Cells were harvested by  
546 centrifugation at 5000 rpm for 25 min at 4°C (rotor 11150, Sigma) and resuspended in  
547 lysis buffer (50 mM Tris-HCl, pH 7.8, 0.5 M NaCl, 1 mM DTT, 25 mM imidazole, 0.1  
548 mg/mL 4-(2-aminoethyl)benzenesulfonyl fluoride (AEBSF), 1 µg/mL leupeptin, 50  
549 µg/mL deoxyribonuclease 1 (DN25, Sigma-Aldrich), 20 mM MgCl<sub>2</sub>). The cells were  
550 lysed using a French® Pressure Cell Press (SLM-Aminco). The lysate was centrifuged  
551 at 10,000 rpm for 30 min at 4 °C (rotor 12165-H, Sigma), and the insoluble fraction was  
552 discarded. The recombinant protein was purified using a HisTrap™ FF crude column  
553 (1 mL, Cytiva) equilibrated with buffer containing 20 mM Tris-HCl, pH 7.8, 0.5 M NaCl,  
554 1 mM DTT, and 25 mM imidazole. *TSPYL5* was eluted with the same buffer containing  
555 1 M imidazole. The eluted fractions were concentrated to a final volume of 500 µL and  
556 further purified by size-exclusion chromatography on a Superdex™ 200 Increase  
557 10/300 GL column equilibrated with 20 mM Tris-HCl, pH 7.8, 0.5 M NaCl, and 1 mM  
558 DTT. Protein concentration was determined using the Bradford assay (Bio-Rad Protein  
559 Assay Dye Reagent), and purity was assessed by SDS-PAGE, followed by staining  
560 with InstantBlue Coomassie Protein Stain (Abcam). The purified protein was dialyzed

561 overnight to a buffer containing 20 mM Tris-HCl, pH 7.8, 0.5 M NaCl, 1 mM DTT, and  
562 10% glycerol. Nano-differential scanning fluorimetry (nanoDSF) was performed using  
563 a Tycho NT.6 instrument (NanoTemper Technologies) in the dialysis buffer at a protein  
564 concentration of approximately 0.8 mg/mL to assess protein folding. Protein aliquots  
565 were stored at  $-80^{\circ}\text{C}$ .

566 *TSPYL5 anti-TR*. The nucleotidic sequence encoding TSPYL5 anti-TR (residues 196-  
567 417 of TSPYL5 FL), modified to include an N-terminal 6x histidine tag followed by a  
568 thrombin cleavage site, was cloned into the pET-28a expression vector and  
569 synthesized by Genecust. The recombinant plasmid was transformed into *Escherichia*  
570 *coli* BL21-Gold cells. Transformed *E. coli* cultures were grown in terrific broth (TB)  
571 supplemented with 50  $\mu\text{g}/\text{mL}$  kanamycin at  $37^{\circ}\text{C}$ . Protein expression was induced by  
572 adding 1 mM isopropyl  $\beta$ -D-1-thiogalactopyranoside (IPTG) when the culture reached  
573 an optical density ( $\text{OD}_{600}$ ) of 0.8. The cultures were incubated overnight at  $37^{\circ}\text{C}$  with  
574 shaking at 130 rpm. Cells were harvested by centrifugation at 5000 rpm for 25 min at  
575  $4^{\circ}\text{C}$  (rotor 11150, Sigma) and resuspended in lysis buffer (50 mM Tris-HCl, pH 7.8, 0.5  
576 M NaCl, 1 mM DTT, 25 mM imidazole, 0.1 mg/mL 4-(2-aminoethyl)benzenesulfonyl  
577 fluoride (AEBSF), 1  $\mu\text{g}/\text{mL}$  leupeptin, 50  $\mu\text{g}/\text{mL}$  deoxyribonuclease 1 (DN25, Sigma-  
578 Aldrich), 20 mM  $\text{MgCl}_2$ ). The cells were lysed using a French<sup>®</sup> Pressure Cell Press  
579 (SLM-Aminco). The lysate was centrifuged at 10,000 rpm for 30 min at  $4^{\circ}\text{C}$  (rotor  
580 12165-H, Sigma), and the insoluble fraction was discarded. The recombinant protein  
581 was purified using a HisTrap<sup>™</sup> FF crude column (1 mL, Cytiva) equilibrated with buffer  
582 containing 20 mM Tris-HCl, pH 7.8, 0.5 M NaCl, 1 mM DTT, and 25 mM imidazole.  
583 TSPYL5 was eluted with the same buffer containing 1 M imidazole. Protein  
584 concentration was determined using the Bradford assay (Bio-Rad Protein Assay Dye  
585 Reagent), and purity was assessed by SDS-PAGE, followed by staining with

586 InstantBlue Coomassie Protein Stain (Abcam). Nano-differential scanning fluorimetry  
587 (nanoDSF) was performed using a Tycho NT.6 instrument (NanoTemper  
588 Technologies) in a mix of wash and elution buffer at a protein concentration of  
589 approximately 6.5 mg/mL to assess protein folding. The purified protein was dialyzed  
590 overnight to a buffer containing 20 mM Tris-HCl, pH 7.8, 0.5 M NaCl, 1 mM DTT, and  
591 10% glycerol. Protein aliquots were stored at  $-80^{\circ}\text{C}$ . Purified proteins was further  
592 analyzed by size-exclusion chromatography on a Superdex™ 200 Increase 10/300 GL  
593 column equilibrated with 20 mM Tris-HCl, pH 7.8, 0.5 M NaCl, and 1 mM DTT for  
594 molecular weight evaluation.

595 *USP7*. *USP7* was ordered from Biotechne (R&D systems) (E-519-025).

596 *MATH domain of USP7*. The nucleotidic sequence encoding the MATH domain,  
597 modified to include an N-terminal 6x histidine tag, was cloned into a pET-28a  
598 expression vector and synthesized by Genecust. The recombinant plasmid was  
599 transformed into *Escherichia coli* Rosetta (DE3) cells. Transformants were grown in  
600 terrific broth (TB) medium supplemented with 50  $\mu\text{g}/\text{mL}$  kanamycin and 34  $\mu\text{g}/\text{mL}$   
601 chloramphenicol at  $37^{\circ}\text{C}$ . When the culture reached an optical density ( $\text{OD}_{600}$ ) of 0.8,  
602 expression of the MATH domain was induced with 1 mM isopropyl  $\beta$ -D-1-  
603 thiogalactopyranoside (IPTG), followed by incubation overnight at  $20^{\circ}\text{C}$  with shaking  
604 at 120 rpm. Cells were harvested by centrifugation at 5000 rpm for 25 min at  $4^{\circ}\text{C}$  (rotor  
605 11150, Sigma), and the cell pellet was resuspended in lysis buffer (50 mM Tris-HCl,  
606 pH 8.5, 300 mM NaCl, 10 mM  $\text{MgCl}_2$ , 5 mM imidazole, 10% glycerol), supplemented  
607 with a protease inhibitor cocktail (cOmplete™ ULTRA Tablets, Mini, EDTA-free,  
608 EASYpack, Roche). The cells were lysed by sonication. The lysate was centrifuged at  
609 10,000 rpm for 30 min at  $4^{\circ}\text{C}$  (rotor 12165-H, Sigma), and the insoluble fraction was  
610 discarded. Beta-mercaptoethanol (1  $\mu\text{L}/\text{mL}$ ) was added to the supernatant. The

611 recombinant protein was purified using HisTrap™ FF crude columns (1 mL, Cytiva)  
612 pre-equilibrated with buffer containing 50 mM Tris-HCl, pH 8.5, 300 mM NaCl, 10 mM  
613 MgCl<sub>2</sub>, 30 mM imidazole, and 10% glycerol. The MATH domain was eluted using 250  
614 mM imidazole. Protein concentration was determined using the Bradford assay (Bio-  
615 Rad Protein Assay Dye Reagent), and purity was assessed by SDS-PAGE, followed  
616 by staining with InstantBlue Coomassie Protein Stain (Abcam). The purified protein  
617 was dialyzed overnight to a buffer containing 50 mM HEPES, pH 7.5, 100 mM NaCl, 1  
618 mM TCEP, and 10% glycerol. Nano differential scanning fluorimetry (nanoDSF) was  
619 performed using a Tycho NT.6 instrument (NanoTemper Technologies) in the dialysis  
620 buffer at a protein concentration of approximately 1.2 mg/mL to confirm proper folding.  
621 Protein aliquots were stored at -80°C.

622 *Peptides.* All the peptides were ordered from ProteoGenix and were acetylated at their  
623 N-termini and amidated at their C-termini.

#### 624 **Protein characterization**

625 *Circular Dichroism.* The buffer for purified full-length TSPYL5 and truncated TSPYL5  
626 was exchanged to 20 mM sodium phosphate, pH 7.4, 200 mM NaF, and 1 mM DTT.  
627 Protein concentrations were determined using the Bradford assay (Bio-Rad Protein  
628 Assay Dye Reagent) for the truncated TSPYL5 and spectrophotometrically (Eppendorf  
629 BioSpectrometer) for the full-length TSPYL5. Both protein samples were diluted in the  
630 assay buffer to a final concentration of 0.2 mg/mL. Circular dichroism (CD)  
631 measurements were conducted at 25°C using a BioLogic MOS-500 spectropolarimeter  
632 (BioLogic, France) with a 1 mm path length quartz cuvette (#110-1-40, Hellma  
633 Analytics). Far-UV spectra were recorded from 190 to 260 nm with an acquisition

634 period of 0.5 s and steps of 1 nm. Five spectra were collected for each sample and  
635 averaged. Data analysis was performed using GraphPad Prism software.

636 *Nano Differential Scanning Fluorimetry.* Purified proteins were analyzed in their  
637 respective dialysis buffers using a Tycho NT.6 instrument (NanoTemper  
638 Technologies), following the standard manufacturer's protocol. Protein samples were  
639 loaded into capillaries and heated to 95°C over a period of 3 min. Fluorescence  
640 emission was monitored at 330 nm and 350 nm, following excitation at 280 nm. The  
641 instrument determined melting temperatures by calculating the derivative of the  
642 fluorescence intensity ratio (350/330 nm) as a function of temperature.

643 *Dynamic Light Scattering.* All samples and buffers were filtered using 0.2 µm filters to  
644 prevent contamination by particles. Dynamic light scattering (DLS) measurements  
645 were conducted using a DynaPro Dynamic Light Scattering Instrument (Wyatt  
646 Technology), and data were processed using DYNAMICS Basic Processing software  
647 (version 7.10.1.21). Samples were placed in specific DLS disposable microcuvettes  
648 (162960; Wyatt technology). Dilutions were performed directly in the cuvette by  
649 removing half of the sample volume and replenishing it with an equal volume of the  
650 storage buffer (20 mM Tris-HCl, pH 7.8, 0.5 M NaCl, 1 mM DTT, and 5% glycerol).  
651 Each sample was measured three times consecutively, with each measurement  
652 comprising five DLS acquisitions of 8 s each, separated by 1-s read intervals.

653 *Negative Staining.* Formvar carbon grids (EMS) were glow discharged using an  
654 ELMO glow discharger for 20 s at 4.5 mA. 3 µl of sample at 0.01mg/ml were applied  
655 to the grid and incubated for 30 s. After removal of the excess liquid, the grids were  
656 stained with 2% uranyl acetate solution (Zhang et al. 2013). After drying, the negative

657 stained grids were imaged using a JEOL1400 microscope equipped with a TVIPS  
658 F416 at 60,000x magnification.

659 *Mass Spectrometry (MALDI-TOF)*. Matrix Assisted Laser Desorption Ionization – Time  
660 of Flight MS was acquired on a Ultraflex extreme enhanced MALDI TOF/TOF-MS system  
661 (Bruker Daltonics, Bremen, Germany) using FlexControl 3.4 acquisition software  
662 (Bruker). For intact mass determinations, 1  $\mu$ L of a 1:1:1 mixture of protein sample, 2.5  
663 DHAP matrix (Bruker) and 2% v/v TFA was spotted in triplicate on an MTP ground  
664 steel plate. After crystallization, spectra were measured in the linear positive ion-mode  
665 within a mass range of 20,000 to 150,000 m/z. Up to 8000 shots were acquired with a  
666 laser repetition rate of 2000 Hz and 200 shots per raster spot. All acquisition methods  
667 were provided by the manufacturer and optimized and calibrated with in-house made  
668 calibration standards (22 to 96 kDa, 4 calibrants). The obtained spectra were analyzed  
669 and processed (peak picking, smoothing and baseline subtraction) with FlexAnalysis  
670 3.4 (Bruker). Finally, the average of the three sample spots was taken to obtain the  
671 measured mass. For top down sequencing (TDS) experiments, 10  $\mu$ L sample was  
672 mixed with 8 M GuHCl and desalted with a C18 ZIPTIP and eluted with a 50 mg/ml  
673 SDHB solution (dissolved in TA50). The eluent was diluted twofold with deionized  
674 water and 1.5  $\mu$ L spotted on an MTP ground steel plate. All TDS experiments were  
675 measured in reflector and ion-positive mode within a range of 500 to 9000 Da with a  
676 by the manufacturer provided optimized acquisition method. Up to 12,000 shots were  
677 manually acquired and the used method was optimized and calibrated with an in-house  
678 made protein (15 kDa). The obtained spectra were processed and analyzed with  
679 FlexAnalysis 3.4 and BioTools 3.2.

680 *Mass Photometry*. Protein mass photometry was performed using a Refeyn OneMP  
681 system (Refeyn Ltd). The buffer, which was filtered prior to use, consisted of 50 mM

682 HEPES, pH 7.5, and 100 mM NaCl. Protein stock solutions at concentrations of 770  
683 nM, 380 nM, and 190 nM were prepared, and 2  $\mu$ L of each stock was directly added to  
684 an 18  $\mu$ L drop of buffer on the measurement surface. Movies were recorded for 60 s  
685 (6000 frames) using the Acquire<sup>MP</sup> software (version 2.1.1; Refeyn Ltd) under standard  
686 acquisition settings. Data analysis was conducted using Discover<sup>MP</sup> software (version  
687 2.1.1; Refeyn Ltd) with default settings. Prior to measurements, contrast-to-mass  
688 calibration was performed using a standard protein mixture with molecular weights of  
689 66, 158, and 670 kDa.

690 *Crosslinking.* The buffer for purified full-length TSPYL5 was exchanged to PBS buffer  
691 (10.1 mM Na<sub>2</sub>HPO<sub>4</sub>, 1.7 mM KH<sub>2</sub>PO<sub>4</sub>, 2.7 mM KCl, 137 mM NaCl, pH 7.6). Proteins  
692 (3.5  $\mu$ M) were incubated with varying concentrations of BS<sup>3</sup> cross-linker  
693 (ThermoFisher, #21580) for 30 min at room temperature. The cross-linking reaction  
694 was quenched by adding 50 mM Tris-HCl, pH 7, and incubating for an additional 15  
695 min. Cross-linked protein samples were mixed with 1 $\times$  Laemmli sample buffer (final  
696 protein concentration of 2.3  $\mu$ M) and heated at 60°C for 10 min. The samples were  
697 then analyzed by SDS-PAGE, and the gels were stained using InstantBlue Coomassie  
698 Protein Stain (Abcam).

699 **Microscale Thermophoresis.** Microscale thermophoresis (MST) measurements were  
700 carried out using a NanoTemper Monolith NT.115 instrument (NanoTemper  
701 Technologies). USP7 was fluorescently labeled with a red dye–N-Hydroxysuccinimide  
702 (NHS) first-generation dye (NanoTemper Technologies), following the manufacturer’s  
703 guidelines. All measurements were performed in premium-treated capillaries  
704 (NanoTemper Technologies) using buffer systems as follows: for TSPYL5 and  
705 truncated TSPYL5, the buffer composition was 95% buffer A (50 mM HEPES, 100 mM  
706 NaCl, 20% glycerol, 1 mM TCEP, 0.01% Tween 20, pH 7.5) mixed with 5% buffer B

707 (20 mM Tris-HCl, 0.5 M NaCl, 10% glycerol, pH 7.6); for peptide measurements, the  
708 buffer consisted of 50 mM HEPES, 100 mM NaCl, 20% glycerol, 1 mM TCEP, 0.01%  
709 Tween 20, pH 7.5. The final concentration of the fluorescently tagged protein was 100  
710 nM. TSPYL5, truncated TSPYL5, or peptides were titrated using a 1:1 serial dilution.  
711 MST measurements were performed with 100% LED power and medium MST power,  
712 with a laser on time of 20 s and a laser off time of 3 s. Thermophoretic movement  
713 patterns were recorded, and dissociation constants ( $K_d$ ) were calculated from the raw  
714 data at 2.5 s of MST on time, in accordance with the manufacturer's instructions, using  
715 MO.Affinity Analysis v2.3 software.

716 **BioLayer Interferometry.** Biolayer interferometry (BLI) measurements were  
717 conducted using an Octet® 96 system (Sartorius). Data were analyzed using FortéBio  
718 Data Analysis software (version 9.0.0.14) for reference subtraction, Savitzky–Golay  
719 filtering, and global fitting of the association and dissociation kinetic parameters.  
720 Proteins were biotinylated using EZ-Link™ NHS-LC-Biotin (Thermo Scientific, #21336)  
721 according to the manufacturer's instructions. Before the biotinylation, protein buffer  
722 was exchanged for PBS buffer through dialysis. NHS-LC-Biotin was prepared as a 10  
723 mM stock solution in DMSO and incubated with protein samples at specific molar ratios  
724 (NHS-LC-Biotin:protein): 20:1 for the MATH domain and TSPYL5, and 1:1 or 0.1:1 for  
725 TSPYL5 optimization experiments. Incubations were conducted for 2 h on ice. Excess  
726 unreacted NHS-LC-biotin was removed by dialysis. The biotinylated proteins were  
727 immobilized onto streptavidin (SA) biosensors (Sartorius, #18-5019) at 2.5 µg/ml  
728 (except for NHS-LC-Biotin:TSPYL5 0.1:1 at 25 µg/ml) in a binding buffer composed of  
729 50 mM HEPES, 100 mM NaCl, 20% glycerol, 1 mM TCEP, and 0.01 % Tween-20, pH  
730 7.5. The interacting protein partner in solution was prepared at varying concentrations  
731 in the same buffer. As a negative control, the NemR protein (Kostyuk et al. 2022) was

732 biotinylated using the same protocol applied to other proteins, with a 20:1 molar ratio  
733 (NHS-LC-Biotin:protein). The biotinylated NemR was immobilized onto the same type  
734 of biosensors at a concentration of 2.5 µg/ml. The sensors were subsequently  
735 subjected to the same experimental conditions as those used for biotinylated MATH  
736 domain or TSPYL5, exposing them to various concentrations of either TSPYL5 or  
737 MATH domain. Binding responses recorded with biotinylated NemR were subtracted  
738 from the corresponding responses obtained with biotinylated MATH domain or  
739 TSPYL5 to eliminate non-specific binding signals. Association and dissociation phases  
740 were recorded in real-time. Data analysis was conducted using FortéBio Data Analysis  
741 software (version 9.0.0.14). Baseline adjustments, reference subtraction, and  
742 Savitzky–Golay filtering were applied, followed by global fitting to determine  
743 association and dissociation kinetic parameters.

744 **Hydrogen Deuterium Exchange Mass Spectrometry.** Hydrogen Deuterium  
745 Exchange Mass Spectrometry HDx-MS experiments were performed using a LEAP  
746 HDx Parralel MF system (Trajan) coupled to an UltiMate 3000 HPLC and an Orbitrap  
747 Fusion Lumos Tribrid Mass Spectrometer (Thermo Scientific). For the interaction  
748 between TSPYL5 and MATH, samples were mixed at a 1:1 ratio at 7.5 µM and stored  
749 at 0°C afterwards. 3.5 µl of proteins were diluted in 56.5 µl of equilibration buffer (5 mM  
750 K<sub>2</sub>HPO<sub>4</sub>, 5 mM KH<sub>2</sub>PO<sub>4</sub> dissolved in H<sub>2</sub>O, pH 7) for non-deuterated controls or in 56.5  
751 µl labelling buffer (5 mM K<sub>2</sub>HPO<sub>4</sub>, 5 mM KH<sub>2</sub>PO<sub>4</sub> dissolved in D<sub>2</sub>O, pD 7) for 15, 60,  
752 300, 900 or 3600 s. 50 µl of the exchange reaction was mixed with 50 µl of quench  
753 buffer (5 mM K<sub>2</sub>HPO<sub>4</sub>, 5 mM KH<sub>2</sub>PO<sub>4</sub>, 4 M urea for TSPYL5 analysis or 6 M urea for  
754 MATH analysis, pH 2.3) at 1°C. 90 µl of the quenched solution was directly injected in  
755 the LC-MS system. Samples were digested using a Nepenthesin-2/Pepsin mixed  
756 column (Affipro, AP-PC-006) at 10°C using a dynamic flowrate of 250-350 µl/min

757 gradient for 2 min for TSPYL5 and a fixed flowrate of 300  $\mu$ l/min for MATH. Digested  
758 peptides were trapped captured on ACQUITY BEH C18 1.7  $\mu$ m VANGUARD Pre-  
759 column (Waters), separated on a C18 5  $\mu$ m 1.0 x 5 mm Vydak column at a flowrate of  
760 25  $\mu$ l/min with a linear gradient of H<sub>2</sub>O/ACN 5-30% before being electrosprayed into a  
761 Orbitrap Fusion Lumos Tribrid Mass Spectrometer (Thermo Scientific). An EThcD  
762 fragmentation was applied for ions +2-+8 and a HCD fragmentation for ions +1 and +2.  
763 Peptides from undeuterated samples were identified using Proteome Discoverer 2.5.  
764 Peptides with XCorr > 2.0 were used as peptides pool for H-D exchange analysis.  
765 Hydrogen-deuterium exchange was calculated using HDExaminer. The deuteration  
766 levels were calculated based on the centroid of theoretical isotopes for all peptides.  
767 Each peptide was visually validated based on retention time and drift time. The results  
768 were further exported and analyzed with Deuterios 2.0 (Lau et al. 2021) using the  
769 peptide and hybrid significance test, as described (Lau et al. 2021). All time points and  
770 conditions were performed in triplicates.

771

## 772 **SUPPLEMENTARY MATERIAL**

773

774 - TSPYL5-USP7-supplementary-material. Supporting data contains figures and  
775 tables describing: Immunoprecipitation experiments in HEK293T cells, mass  
776 spectrometry results (intact mass analysis of TSPYL5 full-length and truncated,  
777 and Top-Down Sequencing Analysis of TSPYL5 truncated), hydrogen-  
778 deuterium exchange mass spectrometry (HDx-MS) analysis of TSPYL5  
779 structure, MATH domain of USP7 purification results, BioLayer Interferometry  
780 optimization, BioLayer Interferometry data for MATH domain binding to  
781 biotinylated TSPYL5 (with different NHS-LC-Biotin:TSPYL5 molar ratio),

782 BioLayer Interferometry data with fitting curves for TSPYL5 full-length or  
783 truncated binding to biotinylated MATH domain, TSPYL5 sequence coverage in  
784 HDx-MS experiments, deuterium exchange results at extended exposure times,  
785 H-D exchange profile of selected peptides, TSPYL5 sequence comparison and  
786 hotspots localization, representation of the three identified interacting regions  
787 on TSPYL5 structure, dynamic light scattering and mass photometry  
788 complementary results, TSPYL5 anti-TR purification results and SEC analysis,  
789 secondary structure predictions based on circular dichroism results, peptides  
790 screened in MST for their binding to USP7 and measured  $K_d$  + Materials and  
791 Methods Tables describing plasmids, primers and antibodies used for Fig. 1 and  
792 Fig. S1.

793

794 - The complete raw data underpinning the results of this study can be obtained  
795 from the corresponding authors upon request.

796

797

## 798 **ACKNOWLEDGMENTS**

799 This work was supported by the Belgian Fonds National de la Recherche Scientifique  
800 (FNRS-EQP 31288018) and a Stichting tegen Kanker grant FAF-F/2018/1208 (to JM  
801 and AD). MA is a Research Fellow of the Belgian Fonds National de la Recherche  
802 Scientifique - FNRS. JM and KW were supported by a VIB grant. EK was supported  
803 by Excellence of Science project No. 30829584 granted to JM. JMP was supported by  
804 a FWO fellowship (1193524N). NP was supported by an Aspirant PhD fellowship from  
805 FSR-FNRS, Belgium. The hydrogen-deuterium exchange mass spectrometry platform

806 was supported by a grant from the Fondation Contre le Cancer awarded to Stefan N.  
807 Constantinescu (Advanced Technology Equipment n°3758).

808 We would like to thank Luis Fernando Durán Armenta for his help with DLS  
809 experiments. We would like to thank Attila Meszaros for helpful discussions during the  
810 preparation of the revised manuscript. We would like to thank the BECM VIB-VUB  
811 cryo-EM imaging facility in Brussels for support during imaging.

812

### 813 **AUTHORS CONTRIBUTIONS**

814 **Marine Ancia:** Conceptualization; methodology; data curation; validation;  
815 investigation; writing – original draft. **Khadija Wahni:** Methodology; data curation;  
816 validation; investigation; supervision. **Joudy Chakrowf:** Peptides screening; protein  
817 production. **Asia El Aakchioui:** Peptides screening; protein production. **Eloïse**  
818 **Claude:** Co-immunoprecipitation assay; data analysis; investigation. **Guillaume de**  
819 **Lhoneux:** Co-immunoprecipitation assay; data analysis; investigation. **Maxime**  
820 **Liberelle:** Methodology; validation; investigation; supervision. **Steven Janvier:** MS  
821 experiments; data analysis. **Ekaterina Baranova:** Structure analysis; validation. **Julia**  
822 **Malo Pueyo:** MP methodology; data curation; validation. **Ariana Jijon Vergara:**  
823 protein production. **Nicolas Papadopoulos:** HDx-MS experiments; data analysis;  
824 investigation. **Clémence Balty:** HDx-MS experiments; data analysis; investigation.  
825 **Jérôme Dejeu:** BLI methodology; validation; investigation; writing – original draft.  
826 **Anabelle Decottignies:** Conceptualization; validation; investigation; writing – review;  
827 project administration; supervision, resources. **Joris Messens:** Conceptualization;  
828 investigation; writing – review; supervision; resources. **Raphaël Frédérick:**

829 Conceptualization; validation; investigation; writing – review; project administration;  
830 supervision; resources.

831

832

## 833 REFERENCES

834

- 835 1. Hanahan D, Weinberg RA (2011) Hallmarks of cancer: The next generation. *Cell*  
836 144(5):646-674.
- 837 2. Claude E, Decottignies A (2020) Telomere maintenance mechanisms in cancer:  
838 Telomerase, alt or lack thereof. *Curr Opin Genet Dev* 60:1-8.
- 839 3. Zhang JM, Zou L (2020) Alternative lengthening of telomeres: From molecular  
840 mechanisms to therapeutic outlooks. *Cell Biosci* 10:30.
- 841 4. Forrest SJ, Georger B, Janeway KA (2018) Precision medicine in pediatric  
842 oncology. *Curr Opin Pediatr* 30(1):17-24.
- 843 5. Episkopou H, Diman A, Claude E, Viceconte N, Decottignies A (2019) Tspyl5  
844 depletion induces specific death of alt cells through usp7-dependent  
845 proteasomal degradation of pot1. *Mol Cell* 75(3):469-482 e466.
- 846 6. Epping MT, Meijer LA, Krijgsman O, Bos JL, Pandolfi PP, Bernards R (2011) Tspyl5  
847 suppresses p53 levels and function by physical interaction with usp7. *Nat Cell*  
848 *Biol* 13(1):102-108.
- 849 7. Silonov S, Smirnov E, Shmidt E, Kuznetsova I, Turoverov K, Fonin A (2024) Insights  
850 into the cellular localization and functional properties of tspyl5 protein.  
851 *International Journal of Molecular Sciences* 25(39).
- 852 8. Dalui S, Dasgupta A, Adhikari S, Das C, Roy S (2022) Human testis-specific y-  
853 encoded protein-like protein 5 is a histone h3/h4-specific chaperone that  
854 facilitates histone deposition in vitro. *J Biol Chem* 298(8):102200.
- 855 9. Jumper J, Evans R, Pritzel A, Green T, Figurnov M, Ronneberger O,  
856 Tunyasuvunakool K, Bates R, Zidek A, Potapenko A et al. (2021) Highly  
857 accurate protein structure prediction with alphafold. *Nature* 596(7873):583-589.
- 858 10. Varadi M, Bertoni D, Magana P, Paramval U, Pidruchna I, Radhakrishnan M,  
859 Tsenkov M, Nair S, Mirdita M, Yeo J et al. (2024) Alphafold protein structure  
860 database in 2024: Providing structure coverage for over 214 million protein  
861 sequences. *Nucleic Acids Res* 52(D1):D368-D375.
- 862 11. Weis DD. 2016. Hydrogen exchange mass spectrometry of proteins:  
863 Fundamentals, methods, and applications.
- 864 12. Lau AM, Claesen J, Hansen K, Politis A (2021) Deuterios 2.0: Peptide-level  
865 significance testing of data from hydrogen deuterium exchange mass  
866 spectrometry. *Bioinformatics* 37(2):270-272.
- 867 13. Oughtred R, Rust J, Chang C, Breitkreutz BJ, Stark C, Willems A, Boucher L,  
868 Leung G, Kolas N, Zhang F et al. (2021) The biogrid database: A  
869 comprehensive biomedical resource of curated protein, genetic, and chemical  
870 interactions. *Protein Sci* 30(1):187-200.
- 871 14. Kim RQ, Sixma TK (2017) Regulation of usp7: A high incidence of e3 complexes.  
872 *J Mol Biol* 429(22):3395-3408.

- 873 15. Ma J, Martin JD, Xue Y, Lor LA, Kennedy-Wilson KM, Sinnamon RH, Ho TF, Zhang  
874 G, Schwartz B, Tummino PJ et al. (2010) C-terminal region of usp7/hausp is  
875 critical for deubiquitination activity and contains a second mdm2/p53 binding  
876 site. *Arch Biochem Biophys* 503(2):207-212.
- 877 16. de Vink PJ, Koops AA, D'Arrigo G, Cruciani G, Spyraakis F, Brunsveld L (2022)  
878 Cooperativity as quantification and optimization paradigm for nuclear receptor  
879 modulators. *Chem Sci* 13(9):2744-2752.
- 880 17. Shen Y, Tu W, Liu Y, Yang X, Dong Q, Yang B, Xu J, Yan Y, Pei X, Liu M et al.  
881 (2018) Tspy1 suppresses usp7-mediated p53 function and promotes  
882 spermatogonial proliferation. *Cell Death Dis* 9(5):542.
- 883 18. Zhang L, Tong H, Garewal M, Ren G (2013) Optimized negative-staining electron  
884 microscopy for lipoprotein studies. *Biochim Biophys Acta* 1830(1):2150-2159.
- 885 19. Kostyuk AI, Tossounian MA, Panova AS, Thauvin M, Raevskii RI, Ezerina D, Wahni  
886 K, Van Molle I, Sergeeva AD, Vertommen D et al. (2022) Hypocrates is a  
887 genetically encoded fluorescent biosensor for (pseudo)hypohalous acids and  
888 their derivatives. *Nat Commun* 13(1):171.

889